01 Jun 2018

Scalable, Hydrophobic and Highly-Stretchable Poly(isocyanurate-Urethane) Aerogels

Sadeq Malakooti

Saman Rostami

Habel Gitogo Churu

Huiyang Luo

et. al. For a complete list of authors, see https://scholarsmine.mst.edu/chem_facwork/2886

Recommended Citation

S. Malakooti and S. Rostami and H. G. Churu and H. Luo and J. Clark and F. Casarez and O. Rettenmaier and S. Daryadel and M. Minary-Jolandan and L. Sotiriou-Leventis and N. Leventis and H. Lu, "Scalable, Hydrophobic and Highly-Stretchable Poly(isocyanurate-Urethane) Aerogels," *RSC Advances*, vol. 8, no. 38, pp. 21214-21223, Royal Society of Chemistry, Jun 2018.
The definitive version is available at https://doi.org/10.1039/c8ra03085e

RSC Advances

PAPER

View Article Online
View Journal | View Issue

Cite this: *RSC Adv.*, 2018, **8**, 21214

Scalable, hydrophobic and highly-stretchable poly(isocyanurate–urethane) aerogels†

Sadeq Malakooti,[a] Saman Rostami,[a] Habel Gitogo Churu,[b] Huiyang Luo,[a] Jenna Clark,‡[a] Fabiola Casarez,‡[a] Owen Rettenmaier,‡[a] Soheil Daryadel,[a] Majid Minary-Jolandan,[a] Chariklia Sotiriou-Leventis,[c] Nicholas Leventis[c] and Hongbing Lu*[a]

Scalable, low-density and flexible aerogels offer a unique combination of excellent mechanical properties and scalable manufacturability. Herein, we report the fabrication of a family of low-density, ambient-dried and hydrophobic poly(isocyanurate–urethane) aerogels derived from a triisocyanate precursor. The bulk densities ranged from 0.28 to 0.37 g cm^{-3} with porosities above 70% v/v. The aerogels exhibit a highly stretchable behavior with a rapid increase in the Young's modulus with bulk density (slope of log–log plot > 6.0). In addition, the aerogels are very compressible (more than 80% compressive strain) with high shape recovery rate (more than 80% recovery in 30 s). Under tension even at high strains (*e.g.*, more than 100% tensile strain), the aerogels at lower densities do not display a significant lateral contraction and have a Poisson's ratio of only 0.22. Under dynamic conditions, the properties (*e.g.*, complex moduli and dynamic stress–strain curves) are highly frequency- and rate-dependent, particularly in the Hopkinson pressure bar experiment where in comparison with quasi-static compression results, the properties such as mechanical strength were three orders of magnitude stiffer. The attained outcome of this work supports a basis on the understanding of the fundamental mechanical behavior of a scalable organic aerogel with potential in engineering applications including damping, energy absorption, and substrates for flexible devices.

Received 10th April 2018
Accepted 31st May 2018

DOI: 10.1039/c8ra03085e

rsc.li/rsc-advances

1. Introduction

Aerogels are low density nanoporous solids containing hierarchical three-dimensional networks of nanoparticles pursued primarily for thermal and acoustic insulations and often for functionalization purposes.[1] Typically, they are prepared using a sol–gel process by supercritical drying of a suitable wet gel.[2] Silica aerogel, as a classical example of a nanostructured porous material, is the most common type of aerogel.[3] However, silica aerogel suffers from severe structural fragility and high production cost (some attempts have been made to reduce its synthesis cost, *e.g.*, ref. 4), which limit its applications.[3] The problem of fragility has been successfully addressed by introducing polymer cross-linked silica aerogels, known as X-aerogels, which contain a post-gelation cross-linking of the silica nanoparticles with a thin polymeric coating.[5] This technology could dramatically improve the mechanical properties of X-aerogels such as mechanical strength and fracture toughness, by a factor of 100 or more with respect to the pristine silica aerogel.

However, this post-gelation process is further adding to the overall production cost of the aerogels. Owing to the substantial improvement in the mechanical properties of X-aerogels with a small amount of polymeric cross-linking agent, it was postulated and later confirmed to consider purely polymeric aerogels with similar X-aerogel nanostructures. For that reason, various polymeric aerogels from different polymeric sources such as polyurea,[6] polyurethane,[7] polyimide[8] and polyamide (KevlarTM-like)[9] have been synthesized. Pure polymeric aerogels resulted to the emergence of new applications such as ballistic armor protection.[10]

Another major obstacle on the aerogel commercialization is the need for supercritical drying. Adopting a scalable nano-manufacturing process to make a balanced combination between the low-density and good mechanical properties without any limitation on the size and dimensions of the product is necessary. Accordingly, the primary intent of this work is to emphasize on the low density nanoporous ambient pressure-dried polymeric aerogels, which would have a lower

[a]*Department of Mechanical Engineering, The University of Texas at Dallas, Richardson, TX 75080, USA. E-mail: hongbing.lu@utdallas.edu; Tel: +1 972 883 4647*
[b]*Department of Mechanical Engineering, LeTourneau University, Longview, TX 75602, USA*
[c]*Department of Chemistry, Missouri University of Science and Technology, Rolla, MO 65409, USA*

† Electronic supplementary information (ESI) available. See DOI: 10.1039/c8ra03085e

‡ NSF Research Experience for Undergraduate (REU) Fellow.

production cost than their supercritical-dried counterparts due to their scalability. Moreover, the mechanical properties of X-aerogels are well investigated (*e.g.*, ref. 11–19) while the polymeric aerogels, specifically those that were prepared under ambient conditions, are less studied (*e.g.*, ref. 6, 20 and 21).

Recently, our co-author has studied a family of supercritical-dried poly(isocyanurate–urethane) aerogels with shape memory capability using triisocyanate derivative of aliphatic hexamethylene diisocyanate (N3300A) and variable-length derivatives of ethylene glycol (EG) diols.[22] Using longer EG-derived diols (*e.g.*, triethylene glycol or tetraethylene glycol), it was shown that the molecular slippage and macroscopic creep for the obtained aerogels are noticeably reduced due to higher hydrogen bonding possibilities between the neighboring urethane branches. Specifically, the triethylene glycol (TEG) based aerogel samples showed an excellent super-elasticity over a wide range of tensile strains. This promising behavior can be exploited at different engineering applications, where high material recovery and vibration damping are required.

Therefore, in this work, using N3300A as precursor and TEG as diol, the poly(isocyanurate–urethane) aerogels are synthesized at low-density with hydrophobic surface properties under ambient conditions to contribute on the synthesis scalability. Subsequently, the thermo-mechanical properties of the obtained aerogels are systematically characterized under both quasi-static (uniaxial tensile and compression testing and dynamic mechanical analysis) and high strain-rate (split Hopkinson pressure bar) loading conditions to consider the realistic service life situations for the synthesized aerogels.

2. Results and discussion

2.1. Synthesis and chemical characterization

The general protocol of the synthesis is adopted from our co-author's recent publication.[22] Fig. 1 shows the synthesis protocol and the reaction pathway to the isocyanurate cross-linking urethane aerogels. Monomers were used at their stoichiometric amounts (triisocyanate : diol = 2 : 3 mol mol^{-1}). Sols were prepared in pure CH_3CN at room temperature. The total monomer concentration was varied between 12% and 15% w/w. The urethane formation was catalyzed by dibutyltin dilaurate (DBTDL) in different amounts varied from 1 : 22 to 1 : 38 mol mol^{-1} ratios relative to N3300A. The exact chemical amounts are tabulated in Table S1 in the ESI.† Prior to gelation, the sols were stirred for 15 min at room temperature. After stirring, the sols were poured into an aluminum mold, coated with a thin layer of silicon rubber, and covered for gelation followed by aging processes, all at room conditions. The samples were monitored every 10–15 min in order to determine the gelation times, and then all samples were aged for 24 h. After aging, wet gels were removed from the molds and washed with a stirred mixture of acetone and small amount of hexylamine (0.3% v/v) for 8 h. Then, the wet gels were washed with pure acetone for 5 times, each for 8 h and finally washed with pentane for another 8 h. The washed wet gels were then dried under ambient conditions. Finally, the samples (*i.e.*, PU aerogels) were heated up in oven at 40 °C for 3 h for further stabilization.

The chemical compositions of the synthesized samples were confirmed with solid-state CPMAS ^{13}C NMR (Fig. 2). It is worth mentioning that the expected N^{13}CO resonance peak of the isocyanate at 122 ppm is missing at the NMR spectrum which indicates the completeness of the reaction. The resonance peaks at 149.3 and 156.3 ppm were associated to the isocyanurate and the urethane carbonyl (–NH(C=O)O–), respectively. The next two peaks at 61.3 and 70.2 ppm were associated to the aliphatic carbons of the diol. The remaining peaks at 27.5 and 42.6 ppm were associated to the –CH_2– groups of N3300A.

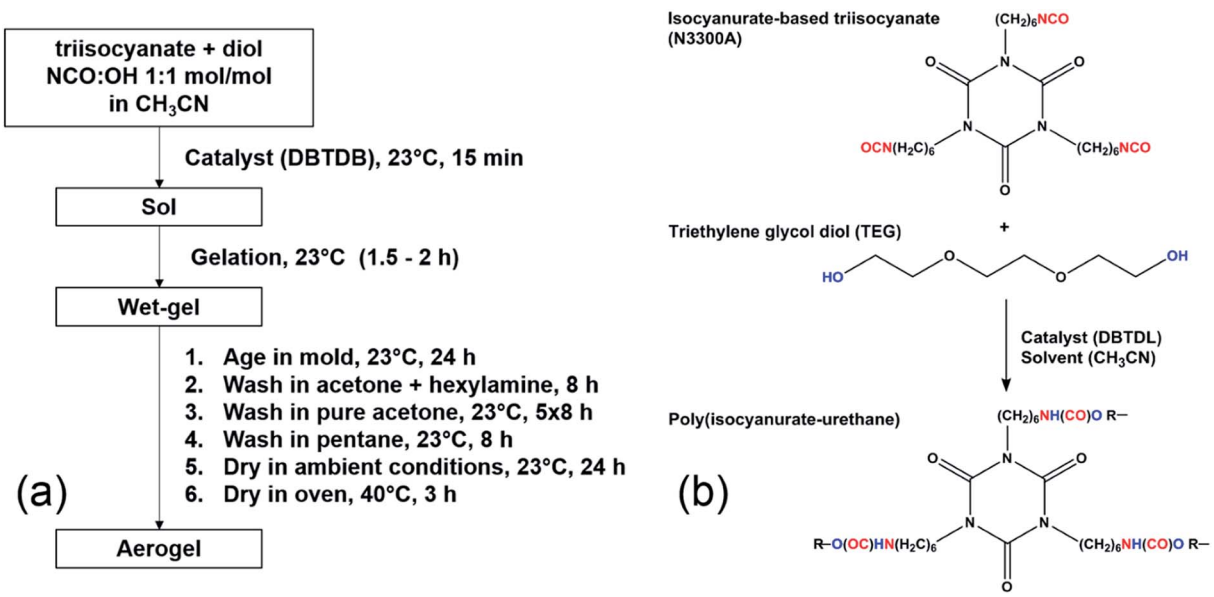

Fig. 1 (a) Synthetic protocol of the PU aerogels; (b) reaction pathway to isocyanurate cross-linking urethane aerogels.

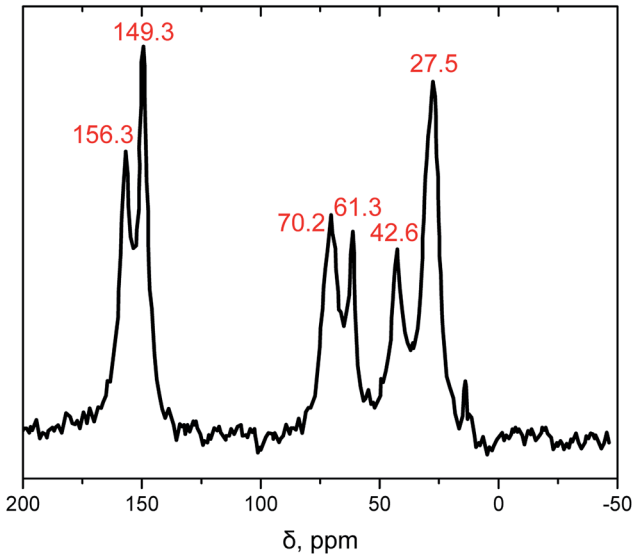

Fig. 2 Typical solid-state CPMAS ^{13}C NMR spectrum of the aerogel.

densities (0.28 and 0.37 g cm^{-3}) are shown here (check Fig. S1 in ESI† for SEM images at all densities). The microstructural evolution with density (*i.e.*, with more concentrated sols) was attributed to spinodal decomposition in combination with slower *vs.* faster gelation: lower concentration sols (yielding aerogels with densities at 0.28 g cm^{-3}) gelled in longer times, 120 min, giving time to the phase-separated polymer to undergo spheroidization. Higher concentrations sols (yielding aerogels with densities at 0.37 g cm^{-3}) gelled faster (90 min) and the observed microstructures were closer to bicontinuous. To induce hydrophobicity, the surfaces of the gels were modified by including a low concentration of hexylamine in the first wash in acetone. Water drop contact angles at different hexylamine concentrations were measured using a goniometer (check Fig. S2 in the ESI†). It was found that the contact angle of water droplet with the gel surface (*i.e.*, ~78° without modification) was increased to 130° with 0.3% v/v concentration as shown in Fig. 3f. Hydrophobicity in aerogels is crucial at the full commercialization phase. It should be noted that the low concentration for the hexylamine is also important since it might affect the gel permeability in solvent exchange followed by drying phases.

Glass transition temperatures (T_g) and material degradation with respect to heat in the PU aerogel samples were then studied through Differential Scanning Calorimetry (DSC) and Thermogravimetric (TGA) analyses and the results for the lowest and highest densities are plotted in Fig. 4 (check Fig. S3 and S4 in the ESI† for all densities). The T_g of all samples (which are also tabulated in Table 1) are either at or below the room temperature (*i.e.*, ~23 °C). Therefore, as expected, all samples are at their rubbery states, which boost their room temperature super-elasticity. Meantime, the TGA results show that all samples are equally resistant to heat and starting to lose mass at about 350 °C. Up to 350 °C, only less than 5% mass-loss, at maximum, was observed for the aerogels. The main decomposition (*i.e.*, more than 90%) occurs between 350 to 500 °C.

2.2. General material properties

The general material properties are summarized in Table 1. Different monomer concentrations led to four distinct densities, ranging from 0.28 to 0.37 g cm^{-3}. The linear shrinkage of the samples relative to the mold size (*i.e.*, the diagonal of the rectangular mold) is between 21 to 25%. All samples' shrinkage happened only during the drying process, which dismisses any probable post polymer reorganization assumptions during the solvent exchanges. The BET surface areas show a drop with increase in bulk density, that agrees with the increase in the aerogel particle sizes. The samples' quality in shape recovery from a sudden contraction was studied by measuring the recovery speed of a cylindrical sample (same dimensions as the compression samples). All samples, approximately expanded on a similar quality with approximate recovery speed of ~1 mm s^{-1} for 80% of the initial contraction.

The obtained rectangular-shape samples were highly flexible. Fig. 3a–c show the typical bending flexibility for one of the samples at 0.28 g cm^{-3} density. Morphology of the samples were also studied with SEM and the images are shown in Fig. 3d and e. Due to the similar trend, morphologies at only two

2.3. Mechanical characterization

Mechanical behavior of the obtained aerogels was investigated through different configurations including quasi-static (*e.g.*, tensile, compression and dynamic mechanical analysis) and high strain-rate loading conditions (*i.e.*, a split Hopkinson

Table 1 The bulk density, porosity, linear shrinkage, recovery speed and glass transition temperature (T_g) data of the synthesized aerogel samples[a]

Name	Bulk density (ρ_b, g cm^{-3})	Porosity[b] (%)	Linear shrinkage[c] (%)	BET surface area[d] (m^2 g^{-1})	Recovery speed[e] (mm s^{-1})	DSC T_g[f] (°C)
PU 1	0.28 ± 0.01	77.20 ± 0.95	24.54 ± 0.56	0.86	0.91	17
PU 2	0.30 ± 0.01	75.58 ± 0.94	23.64 ± 0.60	0.45	0.99	22
PU 3	0.35 ± 0.02	71.50 ± 1.69	22.02 ± 0.55	0.35	1.33	22
PU 4	0.37 ± 0.02	69.88 ± 1.69	22.48 ± 0.71	0.30	1.33	23

[a] Five measurements were made unless otherwise indicated. Skeletal density (ρ_s) is considered to be 1.23 ± 0.005 g cm^{-3}.[22] [b] Porosity = 100 × [(ρ_s − ρ_b)/ρ_s]. [c] Linear shrinkage = 100 × [(mold diagonal − sample diagonal)/mold diagonal]. [d] Single measurement. [e] 80% shape recovery; single measurement. [f] Single measurement.

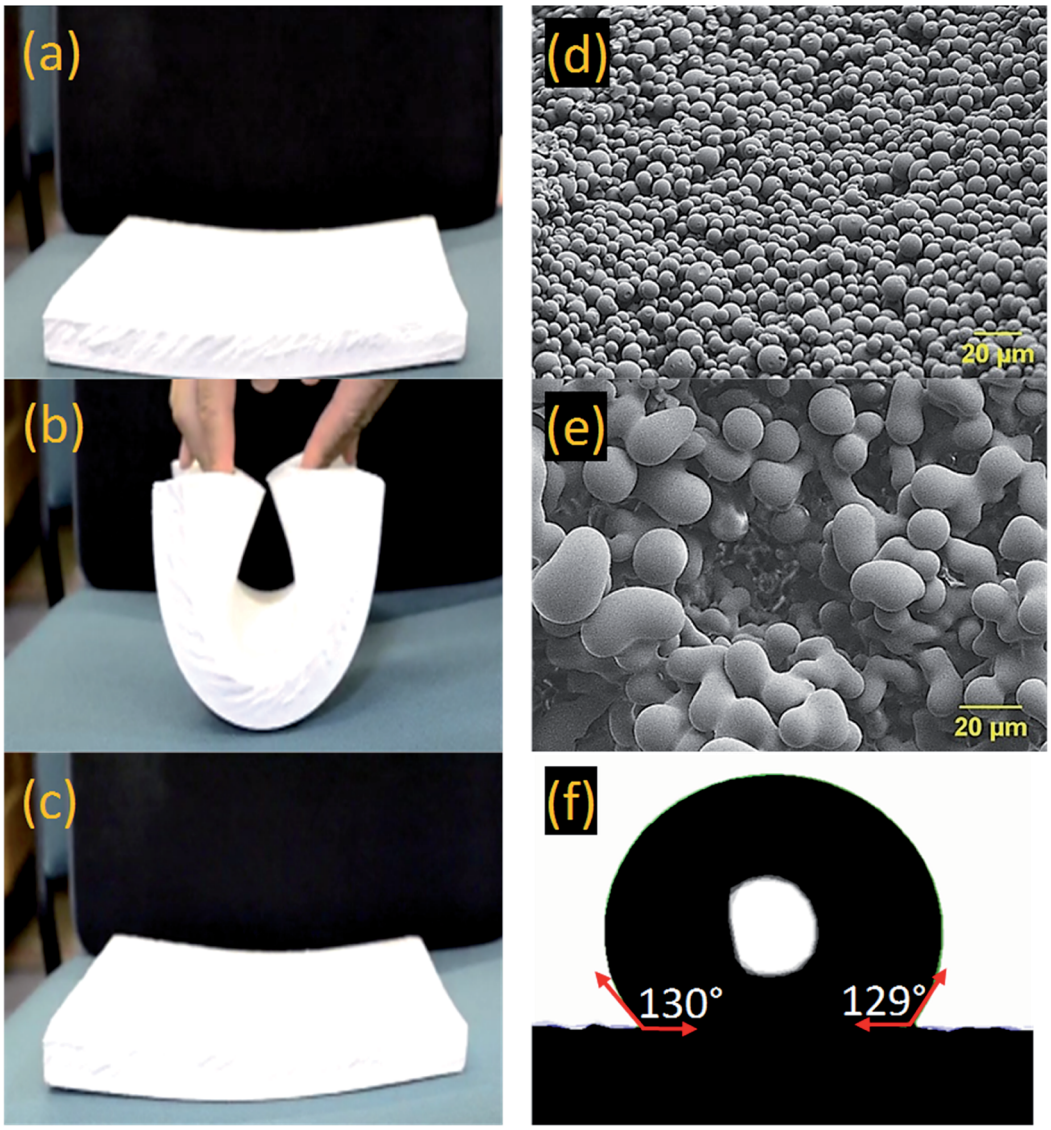

Fig. 3 Typical flexible PU aerogel panel at (a) original, (b) deformed and (c) final shapes at bulk density 0.28 g cm^{-3}; (d) and (e) SEM images of the PU aerogels at bulk densities 0.28 g cm^{-3} and 0.37 g cm^{-3}, respectively; (f) water drop contact angles on the surface of the PU aerogel at bulk density 0.28 g cm^{-3}.

pressure bar experiment). Under quasi-static loading conditions (*i.e.*, strain rate was set less than 0.001 s^{-1}), Fig. 5a shows the typical quasi-static uniaxial tensile test data at room temperature for the aerogel samples at different densities. Linear-elastic behavior is observed for all samples over a wide-range of uniaxial strain (*i.e.*, up to 120% strain). Due to the limited gauge length of the uniaxial tensile test setup (*i.e.*, MTI tensile tester), higher strains than 120% strain was not possible. The variation of Young's modulus *versus* bulk density at room temperature is shown in Fig. 5b. The slope of log–log trend line (*i.e.*, dash line) is calculated to be more than 6, which shows a rapid increase in the modulus with the increase in the density. Digital Image Correlation (DIC) technique concurrent with the tensile tests has been also carried out to measure the 2D displacement and strain fields to obtain the Poisson's ratios of the aerogels. The real-time strain fields along *X* and *Y* directions of the aerogel at 0.28 g cm^{-3} are demonstrated as an example in the ESI materials (*i.e.*, Movie S.1†). The Young's moduli and Poisson's ratios of the aerogels are tabulated in Table 2. It is worth mentioning that the aerogels at lower densities have low Poisson's ratio of 0.22, which is indicative of a small lateral contraction during tension process. In contrast, at higher densities, the Poisson's ratio is also higher to its ultimate value of 0.48 at bulk density 0.37 g cm^{-3}. Also, the wave speed in the aerogels have been estimated using the Young's modulus and bulk density data. The estimated values (11–27 m s^{-1}) are much lower than the speed of sound in open dry air at 20 °C (343 m s^{-1}), inferring that the aerogels are expected to be also a good sound attenuator.

In addition to tensile test, different cyclic compression scenarios have been tested on the aerogels. Due to similar behaviors, only lowest and highest density samples were

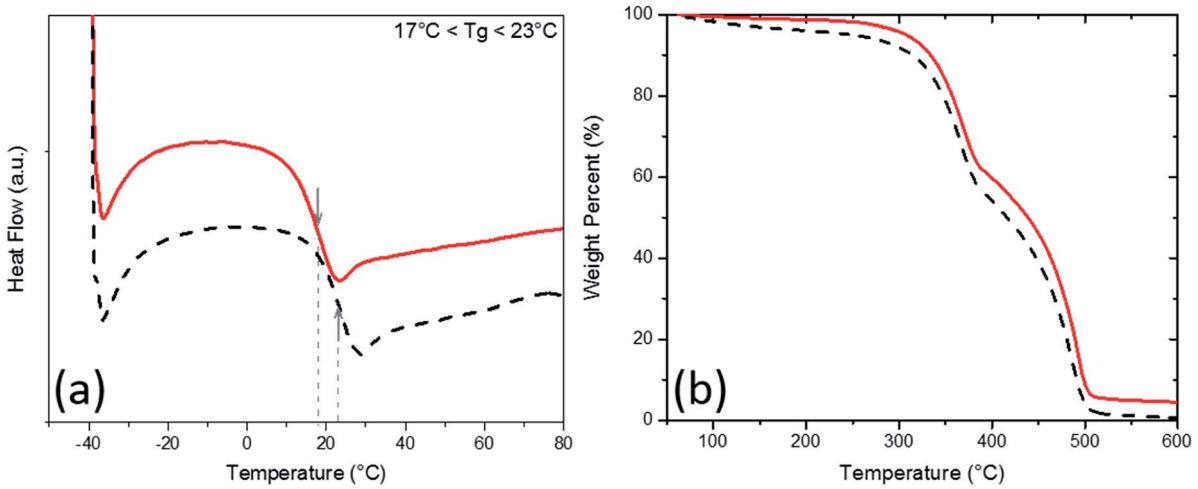

Fig. 4 (a) Differential scanning calorimetry and (b) thermogravimetric analysis of PU aerogels at bulk densities 0.28 g cm^{-3} (solid line) and 0.37 g cm^{-3} (dash line).

considered for these tests. At first, in order to assess the aerogels' stability and resilient property under cyclic loadings, cyclic loading–unloading compression test at 50% strain was conducted and results for two densities are shown in Fig. 5c and d. For each cycle, the starting point is the same and equal to the initial sample length. Therefore, for both densities, a decent strain recovery can be shown after finishing of a cycle and before starting of the next one. The main drop in the stress at both densities occurs after the first cycle mainly due to possible crack initiations. The remaining drops can be associated to the dissipations due to microstructural buckling, adhesion and friction between polymeric branches and further crack formation. Quantitatively, energy dissipation and maximum stress at each cycle can be considered as the key functions for the aerogels' energy absorption capabilities (see Fig. 5e and f). The patterns of maximum stress at both densities are very similar, where after five consecutive cycles, the values are nearly 10 and 45 kPa for low and high-density aerogels, respectively. The normalized absorption energies with respect to the first cycle absorption energy are shown in Fig. 5f. Similar to the maximum stress behavior, the energy dissipation behavior at consecutive loading cycles for both densities are fairly similar. The low-density sample stays at ~60% of its initial dissipation capability, after five consecutive cycles, while the high-density sample at ~80% of its first cycle. It is worth mentioning that the first cycle dissipation energy was tripled with only 25% increase in the bulk density of the aerogels (see Fig. 5f).

In the next compression experiment, the samples are compressed at four-stepped cycles at different strain amplitudes of 20, 40, 60 and 80% in sequence. In contrast with the previous compression test, the starting point of each cycle is at the end of the unloading part of the pervious cycle. Fig. 6 shows the stress–strain curves of the PU aerogels with loading–unloading–reloading cycles at bulk densities 0.28 and 0.37 g cm^{-3}. A nonlinear recovery can be shown for all unloading curves. A decent recovery even at 80% strain exists for the PU aerogels especially at bulk density 0.37 g cm^{-3}, which indicates a high level of compressibility for this class of aerogels. Each succeeding loading curve rises back to the maximum stress point of the preceding cycle, indicating a strong strain memory effect in the aerogels. Additionally, due to this memory effect, a negative slope (stiffness) for the stress–strain curve at the beginning of each unloading zone can be observed. The reloading curves do not follow the loading curves, resulting in a hysteresis loop for each cycle. Both samples started to experience the densification effects at higher strain levels (*i.e.*, ~above 70% strain).

Complex modulus and loss tangent of the PU aerogels using Dynamic Mechanical Analysis (DMA) in compression mode were studied at different temperatures and frequencies (Fig. 7). As it is expected, high-density sample has a higher complex modulus than the low-density sample. The modulus difference is more noticeable at low temperatures, where the materials are stiff (*e.g.*, high-density storage and loss moduli are about 3 and 10 times higher than low-density corresponding values at −50 °C, respectively). At low temperatures, both storage and loss moduli are about 1000 times higher than their respective high-temperature values for both densities. Also, storage moduli are about 100 times bigger than the loss moduli at all temperatures for both densities. Moreover, Fig. 7c indicates the loss tangent (*i.e.*, the ratio of loss modulus to storage modulus) behavior of the samples at different temperatures and frequencies with a peak corresponding to the glass transition temperature (*i.e.*, DMA T_g). Here, multi-frequency analysis allows one to study the glass transition shift in the aerogel samples. Generally, the DMA T_gs are in agreement with DSC T_gs. The DMA T_gs are shifting to higher temperatures with increasing frequency. At higher frequencies, the molecular relaxations can only occur at higher temperatures, which means glass transition should start at higher temperatures as well. The T_g has increased about 5 °C at both densities with frequency increase from 1 to 10 Hz.

High strain-rate mechanical properties of the aerogels have been also studied by means of a long split-Hopkinson pressure

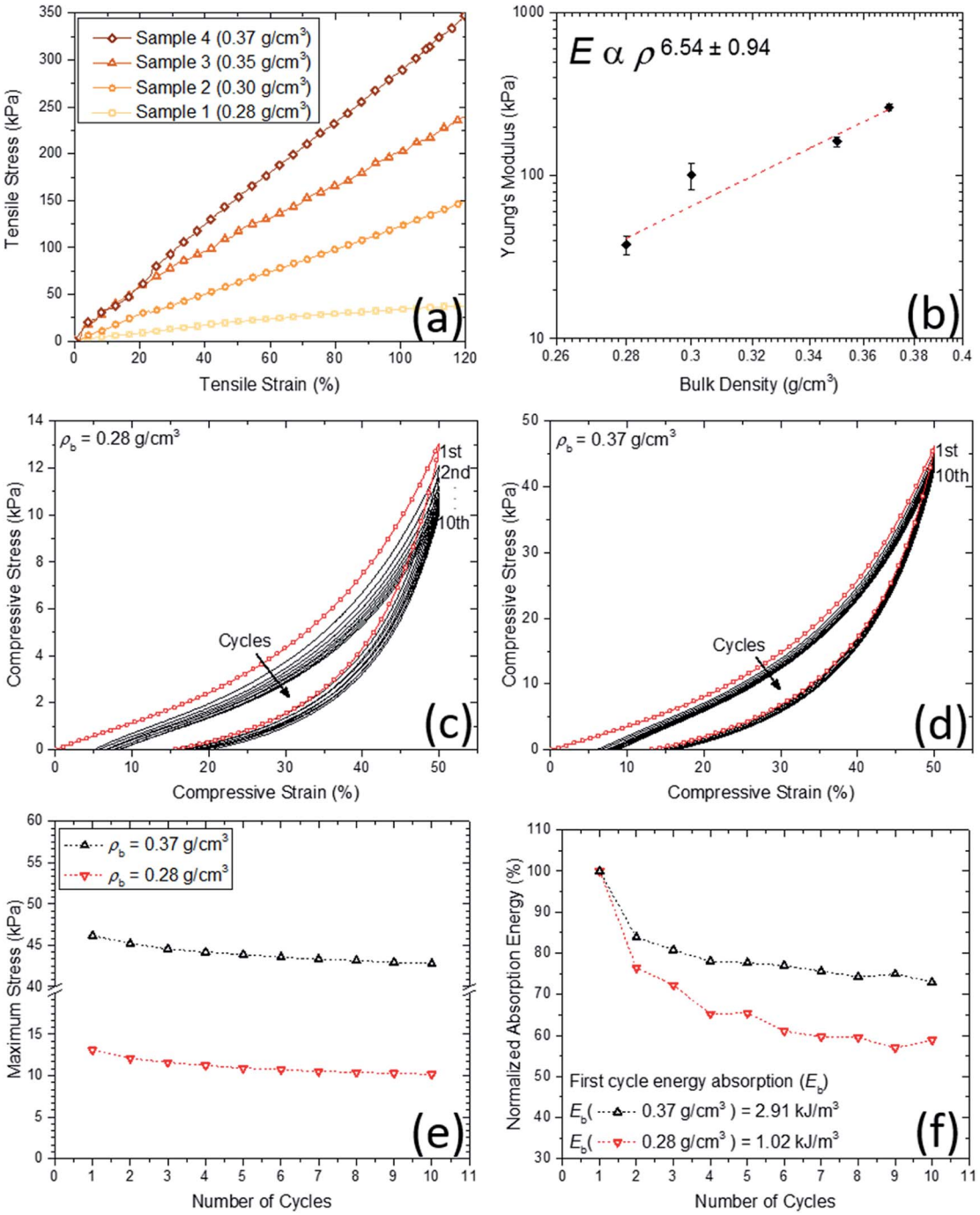

Fig. 5 (a) Typical quasi-static uniaxial tensile stress–strain responses of PU aerogels at different bulk densities; (b) power–law relationship of Young's modulus with bulk density of the PU aerogels; (c) and (d) cyclic quasi-static load–unload compression testing at 50% strain of PU aerogels at bulk densities 0.28 and 0.37 g cm^{-3}, respectively; (e) maximum stress and (f) normalized absorption energy during 10 consecutive cycles for PU aerogels at bulk densities 0.28 and 0.37 g cm^{-3}.

bar (SHPB) under ambient conditions. Specifically, the effects of different strain rates on the stress–strain curves of aerogels at two different densities were considered. Fig. 8 shows the compressive stress–strain curves of PU aerogels at high strain rates. It is notable that each stress–strain curve in Fig. 8 represents the mean value of six experiments at strain rates close to the target strain rates (a reproducible identical strain rate is a very difficult task in SHPB experiment). The actual experimental data at different strain rates are depicted in Fig. S5 of the ESI.† Dramatic change in the stress–strain relationships of the aerogels at both densities are observed at different strain-rates. The general compressive behavior contains of an initial linear elastic region, followed by yielding (which does not exist at the quasi-static responses) and hardening associated with the

Table 2 Room temperature quasi-static Young's modulus, Poisson's ratio and speed of wave propagation data of the synthesized aerogel samples

Name	Young's modulus (kPa)	Poisson's ratio	Wave speed[a] (m s^{-1})
PU 1	37.86 ± 5.24	0.22 ± 0.01	11.63
PU 2	100.90 ± 18.82	0.22 ± 0.01	18.34
PU 3	163.02 ± 11.54	0.35 ± 0.01	21.58
PU 4	265.19 ± 13.40	0.48 ± 0.02	26.31

[a] Wave speed = $\sqrt{\text{Young's modulus/bulk density}}$.

compaction of material pores. The aerogel's Young's modulus, strength and maximum strain reached in each experiment are listed in Table 3. The materials are showing strong strain-rate sensitivity especially in comparison with quasi-static compression tests (*i.e.*, Fig. 5c and d and 6), where mechanical properties are orders of magnitude smaller. At the high strain-rates, all samples failed at 50–80% strain levels with an enhancement in the stiffness with an increase in the strain-rate.

3. Experimental

3.1. Materials

All materials were commercially sourced and used without further processing. The isocyanurate node (*i.e.*, Desmodur N3300A) was generously donated by Covestro LLC (Pittsburg, PA). The diol, triethylene glycol (TEG), and the solvents (anhydrous acetone and anhydrous acetonitrile) were sourced from Fisher Scientific (Hampton, NH). The catalyst, dibutyltin dilaurate (DBTDL), was purchased from Acros Organics. An aluminum container with the dimensions of 70 cm × 70 cm × 5 cm coated with a thin layer of silicon rubber was used as the mold.

3.2. Synthesis of poly(isocyanurate–urethane) aerogels

In a typical synthesis, 30 mmol of N3300A with 45 mmol of TEG were dissolved in an anhydrous acetonitrile (exact amounts are listed in Table S1 of the ESI†). The solution was stirred for 10 min at room conditions. Then the catalyst (DBTDL) was added to the solution. The resulting solution was stirred for another 15 min and poured into an aluminum mold. The mold was covered tightly with aluminum foil for the entire gelation and aging processes. For different densities, the gelation time was varied between 1.5 to 2 h. The aging time was set to 24 h. After aging, the wet gel was washed with a mixture of anhydrous acetone and small amount of hexylamine (0.3% v/v) for 8 h. Then, the hexylamine modified wet gel was washed with pure anhydrous acetone for 5 times (each for 8 h) and finally washed with pentane for another 8 h. The amount of solvent at each washing step was equal to four times of the volume of the wet gel. The washed wet gel was dried under ambient conditions for 24 h. Finally, the samples, which are called PU aerogel, were heated up in oven at 40 °C for 3 h for further stabilization.

3.3. Methods

3.3.1. Chemical characterization. Solid-state CPMAS ^{13}C NMR spectra were obtained with samples cut into small pieces

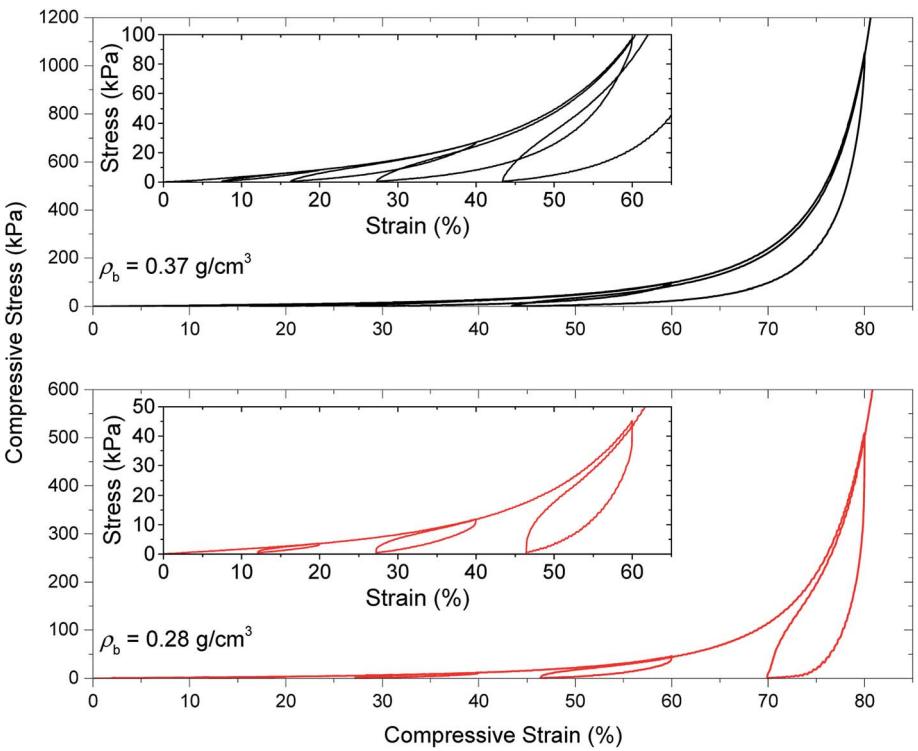

Fig. 6 Quasi-static load–unload–reload compression testing of PU aerogels at bulk densities of 0.28 and 0.37 g cm^{-3}.

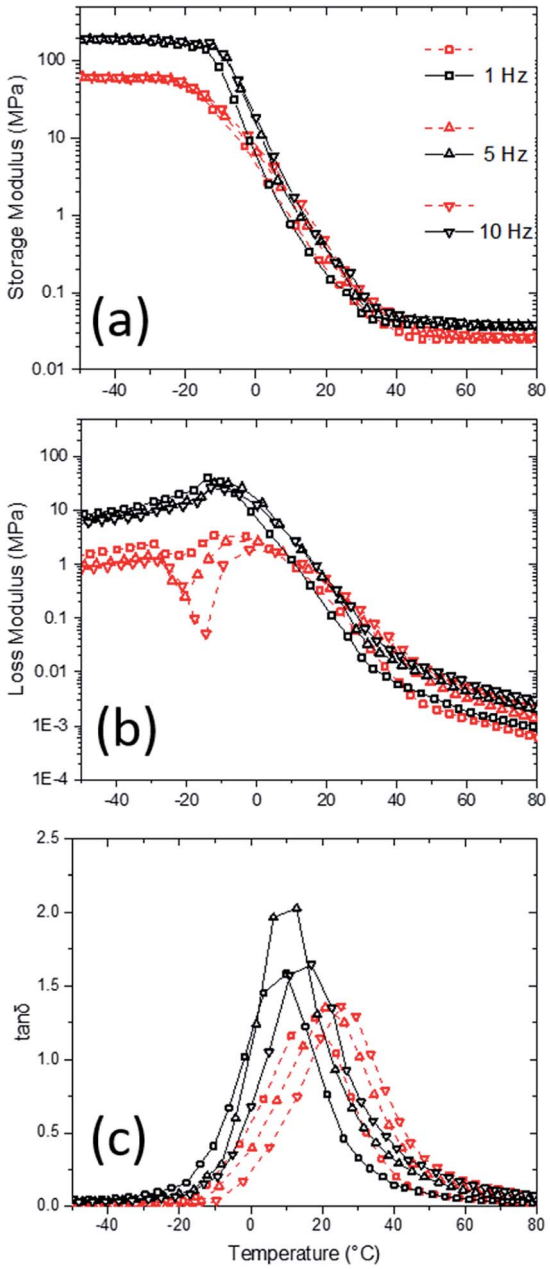

Fig. 7 Dynamic mechanical analysis in compression mode ((a): storage modulus, (b): loss modulus, and (c): tan delta) of PU aerogels at bulk densities 0.28 (dash line) and 0.37 (solid line) g cm^{-3} at different temperatures and frequencies.

on a Bruker Avance III 400 MHz spectrometer with a carbon frequency of 100 MHz using a 7 mm Bruker MAS probe at a magic angle spinning rate of 5 kHz with broad-band proton suppression and the CP TOSS pulse sequence. The Total Suppression of Spinning Sidebands (TOSS) pulse sequence was applied by using a series of four properly timed 180° pulses on the carbon channel at different points of a cycle before acquisition of the FID, after an initial excitation with a 90° pulse on the proton channel. The 90° excitation pulse on the proton and the 180° excitation pulse on carbon were set to 4.2 and 10 μs, respectively. A contact time of 2 ms was used for cross-polarization.

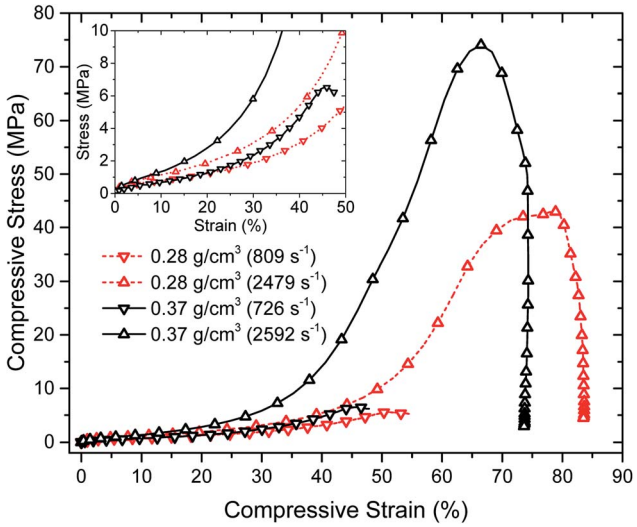

Fig. 8 Room temperature compressive behavior of PU aerogels at bulk densities 0.28 (dash line) and 0.37 (solid line) g cm^{-3} at high strain rates.

3.3.2. Physical characterization. Bulk densities (ρ_b) were determined from the weight and the physical dimensions of the samples. Skeletal density (ρ_s) is considered to be 1.23 ± 0.005 g cm^{-3} according to our co-author previous measurements.[22] Hydrophobicity of the aerogel surfaces were studied by means of static contact angle measurements, through a drop shape analysis system, using a goniometer (KRUSS, DSA30) and water droplets of 11.5 μL volume. Surface areas by the Brunauer–Emmett–Teller (BET) method were determined by nitrogen sorption porosimetry using a Micromeritics ASAP 2020 surface area and pore distribution analyzer.

3.3.3. Structural characterization. SEM Images were taken using ZEISS SUPRA-40 FE-SEM (Carl Zeiss Microscopy GmbH, Germany) with EHT set to 3 kV and occasionally 5 kV. Samples for SEM images were fixed onto a copper tape. In order to reduce charging artifact, prior to SEM imaging, samples were coated with ~7 nm Gold using Hummer-VI sputtering tool (Anatech USA, Union City, CA).

3.3.4. Thermal characterization. DSC was performed on a Mettler Toledo (Columbus, OH) DSC 1 in a 40 μL aluminum crucible. Samples were heated from room temperature to 130 °C, cooled to −40 °C, and subsequently heated to 200 °C. All heating and cooling rates were fixed at 10 °C min^{-1}. Tests were conducted in an N_2 atmosphere. Only the last heating ramp is shown in data, and the T_g is denoted as the midpoint of the transition. TGA analysis was performed on a TGA/DSC 1 STARe System (Mettler Toledo AG Analytical, Switzerland) with a temperature range of 30–700 °C and a ramp rate of 10 °C min^{-1} under an N_2 atmosphere.

3.3.5. Mechanical characterization. Quasi-static uniaxial tensile properties were measured using a MTI microtensile stage (MTI Instruments, Inc., Albany, NY) with 50 lb load cell (0.2% load accuracy) and 20 nm resolution for linear scale accuracy. Dogbone-shaped samples were prepared with 3 mm thickness, 4 mm reduced section width and 11 mm gauge

Table 3 Room-temperature high strain-rate Young's modulus, strength and maximum strain reached data of the synthesized aerogel samples at two different densities

Name	Strain rate (s^{-1})	Young's modulus (MPa)	Strength (MPa)	Maximum strain reached (%)
PU1	809 ± 43	15.2 ± 3.5	5.6 ± 1.7	51.0 ± 2.6
PU1	2479 ± 122	23.3 ± 5.5	44.0 ± 9.7	75.9 ± 4.5
PU4	726 ± 32	11.0 ± 4.0	6.6 ± 3.5	46.2 ± 1.8
PU4	2592 ± 114	28.7 ± 9.8	77.0 ± 17.7	66.7 ± 6.1

length. The strain rate was set to 0.001 s^{-1}. The samples were then sanded to remove all sharp edges or cracks that might cause stress concentrations. Three samples at each density were tested. In order to measure the Poisson's ratios of the aerogels, a random speckle pattern was generated on the surface under observation of the tensile test sample (which is naturally synthesized in white color) using a quick drying black ink. DIC technique, a non-contact full-field deformation measurement method, was used to measure the surface deformations using commercially available 2D SpeckleTrack software (Framingham, MA). During the tensile tests, a series of digital images were taken every 6 s using a Nikon camera (Model D7100) kept at a fixed position and normal to the samples.

Quasi-static compression tests were performed on an Instron mechanical testing system (Instron Inc., Model 5969, Norwood, MA) with 500 N load cell (with accuracy of 0.5% of the reading). The compression rate was set to 0.5 mm min^{-1}. Cylindrical-shaped samples with 20 mm diameter and 20 mm height were drilled out from a larger PU aerogel sample.

DMA was performed on a Mettler Toledo (Columbus, OH) DMA/SDTA861e. Cylindrical-shaped samples with 17 mm diameter and 4 mm thickness were prepared. The deformation mode was in compression. Samples were inserted at room temperature and cooled to −50 °C. The sample was then heated to 100 °C at a rate of 2 °C min^{-1} while undergoing deformation at 1, 5 and 10 Hz. The deformation was force limited to 5 N, with a 200 μm offset (5% strain) and oscillating deformation amplitude of 20 μm (0.5% strain).

Compression experiments at high strain rates (800–2500 s^{-1}) were conducted on a long split-Hopkinson pressure bar (SHPB) under ambient conditions. The SHPB consists of 304 L stainless steel striker bar, a 304 L stainless steel incident bar (8.810 mm length, 19 mm outer diameter), a solid 7075-T651 aluminum transmission bar (3660 mm long, 19 mm in diameter), and a strain data acquisition system. Disk-shaped PU samples (5–7 mm in thickness and 9.6–10 mm in diameter) were sandwiched between the incident and transmission bars. The use of an aluminum transmission bar took advantage of the low Young's modulus of aluminum (∼1/3 of steel) to reach high signal-to-noise ratios for the weak transmitted signal through aerogels[7,23,24] and attain similar functions to those accessible with hollow transmission steel tubes.[10,14,25] A Cu disk pulse shaper (1.6 mm-thick, 7.4 mm in diameter) was used to reach a dynamic stress equilibrium state and constant strain rates, which is necessary for a valid SHPB experiment.[17,26] The working principle of SHPB has been well documented in the literature, including formulas for the stress, strain, and strain rate for a valid experiment.[27–29]

4. Conclusions

Herein, a mass-producible synthetic protocol for the preparation of a hydrophobic polymeric aerogel with rubber-like elasticity has been examined from polymerization of an isocyanurate precursor (N3300A). Large patches of aerogels with densities as low as 0.28 g cm^{-3} and porosities as high as ∼77% were prepared and their mechanical properties were systematically characterized at different loading and environmental conditions. These aerogels showed high thermal stability up to 300 °C with only less than 3% mass-loss while the glass transition was below or at room temperature at all densities. Notable dependencies in the mechanical behavior of the obtained aerogels have been observed with respect to bulk density and strain-rate. For instance, the aerogels were linear-elastically stretchable without any yielding up to at least 120% tensile strain. Also, the stiffness of the aerogels in the quasi-static uniaxial tension tests was significantly increased with respect to the increase in the bulk density, an increase that to our knowledge is not common among other similar aerogel counterparts. Furthermore, the aerogels were studied under cyclic loading-unloading compression tests, which pointed to a very repeatable and stable behavior with a negligible drop in maximum stresses and absorption energies after the second cycle. Dynamic properties of the aerogels have been also measured using multiple-frequency dynamic mechanical analysis at various temperatures and a split Hopkinson pressure bar system. The compressive properties at high strain rates were increased by orders of magnitude with respect to the quasi-static counter-results, indicating high strain rate dependency in this class of aerogels. Finally, it is anticipated that these materials, due to their exciting physical and mechanical properties (*e.g.*, super-elasticity at low density), can be mass-produced with a minimum technical difficulty at a reasonable price (*e.g.*, no need for supercritical drying) to be used for different multifunctional applications in a near future.

Contributions

S. Malakooti and H. Lu conceived the study. N. Leventis, C. Sotiriou-Leventis, H. G. Churu, S. Malakooti and H. Lu designed the synthesis. S. Malakooti, J. Clark, F. Casarez and O. Rettenmaier synthesized and characterized the samples. S. Daryadel,

S. Malakooti, S. Rostami and M. Minary-Jolandan performed the imaging and tensile tests and analyzed the results. S. Rostami carried out the DIC experiments and analyzed the results. H. Luo performed the SHPB experiment and analyzed the results. S. Malakooti performed all other thermal and mechanical experiments and analyzed the results. S. Malakooti and H. Lu wrote the manuscript. All authors reviewed and revised the manuscript.

Conflicts of interest

There are no conflicts to declare.

Acknowledgements

We thank Mr J. Salazar for the assistance with the DMA experiments, and Mrs N. Mohammadi for the static contact angle measurements. Also, S. M. thanks Mr R. Swamy and Mr T. Haines for their help on the material preparations. In addition, the support by NSF CMMI-1636306, CMMI-1661246, and CMMI-1726435, and Nashi-Tech New Materials, Inc. China is acknowledged. N. L. and C. S.-L. thank the Army Research Office under W911NF-14-1-0369. H. L. also thanks the Luis A. Beecherl Jr. Chair for additional support and Covestro LLC (formerly Bayer Corporation U.S.A.) for the supply of Desmodur N3300A.

References

1 A. C. Pierre, in *Aerogels Handbook*, Springer New York, New York, NY, 2011, pp. 3–18.
2 A. C. Pierre and G. M. Pajonk, *Chem. Rev.*, 2002, **102**, 4243–4266.
3 A. C. Pierre and A. Rigacci, in *Aerogels Handbook*, Springer New York, New York, NY, 2011, pp. 21–45.
4 H. Schäfer, B. Milow and L. Ratke, *RSC Adv.*, 2013, **3**, 15263–15272.
5 N. Leventis, C. Sotiriou-Leventis, G. Zhang and A.-M. M. Rawashdeh, *Nano Lett.*, 2002, **2**, 957–960.
6 N. Leventis, C. Sotiriou-Leventis, N. Chandrasekaran, S. Mulik, Z. J. Larimore, H. Lu, G. Churu and J. T. Mang, *Chem. Mater.*, 2010, **22**, 6692–6710.
7 C. Chidambareswarapattar, P. M. McCarver, H. Luo, H. Lu, C. Sotiriou-Leventis and N. Leventis, *Chem. Mater.*, 2013, **25**, 3205–3224.
8 C. Chidambareswarapattar, L. Xu, C. Sotiriou-Leventis, N. Leventis, W. M. Skiff, C. E. Tattershall, A. K. Kalkan, J. T. Mang, C. Sotiriou-Leventis and N. Leventis, *RSC Adv.*, 2013, **3**, 26459–26469.
9 N. Leventis, C. Chidambareswarapattar, D. P. Mohite, Z. J. Larimore, H. Lu and C. Sotiriou-Leventis, *J. Mater. Chem.*, 2011, **21**, 11981–11986.
10 H. Lu, H. Luo and N. Leventis, in *Aerogels Handbook*, Springer New York, New York, NY, 2011, pp. 499–535.
11 G. W. Scherer, D. M. Smith, X. Qiu and J. M. Anderson, *J. Non-Cryst. Solids*, 1995, **186**, 316–320.
12 A. Katti, N. Shimpi, S. Roy, H. Lu, E. F. Fabrizio, A. Dass, L. A. Capadona and N. Leventis, *Chem. Mater.*, 2006, **18**, 285–296.
13 S. Roy and A. Hossain, in *Multiscale Modeling and Simulation of Composite Materials and Structures*, ed. Y. W. Kwon, D. H. Allen and R. Talreja, Springer, 2008, p. 463.
14 H. Luo, G. Churu, E. F. Fabrizio, J. Schnobrich, A. Hobbs, A. Dass, S. Mulik, Y. Zhang, B. P. Grady, A. Capecelatro, C. Sotiriou-Leventis, H. Lu and N. Leventis, *J. Sol-Gel Sci. Technol.*, 2008, **48**, 113–134.
15 C. Wingfield, A. Baski, M. F. Bertino, N. Leventis, D. P. Mohite and H. Lu, *Chem. Mater.*, 2009, **21**, 2108–2114.
16 N. Leventis, C. Sotiriou-Leventis, S. Mulik, A. Dass, J. Schnobrich, A. Hobbs, E. F. Fabrizio, H. Luo, G. Churu, Y. Zhang and H. Lu, *J. Mater. Chem.*, 2008, **18**, 2475–2482.
17 H. Luo, H. Lu and N. Leventis, *Mech. Time-Depend. Mater.*, 2006, **10**, 83–111.
18 G. Churu, B. Zupančič, D. Mohite, C. Wisner, H. Luo, I. Emri, C. Sotiriou-Leventis, N. Leventis and H. Lu, *J. Sol-Gel Sci. Technol.*, 2015, **75**, 98–123.
19 S. Mulik, C. Sotiriou-Leventis, G. Churu, H. Lu and N. Leventis, *Chem. Mater.*, 2008, **20**, 5035–5046.
20 R. W. Pekala, C. T. Alviso and J. D. LeMay, *J. Non-Cryst. Solids*, 1990, **125**, 67–75.
21 C. Tan, B. M. Fung, J. K. Newman and C. Vu, *Adv. Mater.*, 2001, **13**, 644–646.
22 S. Donthula, C. Mandal, T. Leventis, J. Schisler, A. M. Saeed, C. Sotiriou-Leventis and N. Leventis, *Chem. Mater.*, 2017, **29**, 4461–4477.
23 D. P. Mohite, S. Mahadik-Khanolkar, H. Luo, H. Lu, C. Sotiriou-Leventis and N. Leventis, *Soft Matter*, 2013, **9**, 1516–1530.
24 D. P. Mohite, S. Mahadik-Khanolkar, H. Luo, H. Lu, C. Sotiriou-Leventis and N. Leventis, *Soft Matter*, 2013, **9**, 1531–1539.
25 H. Luo, Y. Zhang, B. Wang and H. Lu, *Journal of Offshore Mechanics and Arctic Engineering*, 2010, **132**, 021301.
26 H. Luo, S. Roy and H. Lu, *Compos. Sci. Technol.*, 2012, **72**, 159–166.
27 D. J. Frew, M. J. Forrestal and W. Chen, *Exp. Mech.*, 2002, **42**, 93–106.
28 G. T. Gray, *Classic Split-Hopkinson Pressure Bar Testing*, ASM International, Materials Park, Ohio, 2000.
29 B. A. Gama, S. L. Lopatnikov and J. W. Gillespie, *Appl. Mech. Rev.*, 2004, **57**, 223.